Korean J. Chem. Eng., 40(4), 722-726 (2023)
DOI: 10.1007/s11814-022-1374-y

pISSN: 0256-1115
eISSN: 1975-7220

RAPID COMMUNICATION

Dopant-induced red emission, paramagnetism, and hydrogen evolution of diluted magnetic semiconductor ZnS : Eu nanoparticles

Siva Pratap Reddy Mallem*,‡, Peddathimmula Puneetha,‡, Kalupudi Subramanyam***, Varra Rajagopal Reddy****, Dong-Yeon Lee**, Young Lae Kim*****,†, Sung Jin An******,†, and Kwi-Il Park*******,†**

*Advanced Material Research Center, Kumoh National Institute of Technology, Gumi 39177, Korea
**Department of Robotics and Intelligent Machine Engineering/College of Mechanical and IT Engineering, Yeungnam University, Gyeongsan 38541, Korea
***Department of Physics, Government Degree College, Jaggampeta 533435, East Godavari, India
****Department of Physics, Sri Venkatewara University, Tirupati 517501, India
*****Department of Electronic Engineering, Gangneung-Wonju National Univeristy, Gangneung 25457, Korea
******Department of Materials Science and Engineering, Kumoh National Institute of Technology, Gumi 39177, Korea
*******School of Materials Science and Engineering, Kyungpook National University, Daegu 41566, Korea
(*Received 29 August 2022 • Revised 23 November 2022 • Accepted 11 December 2022*)

Abstract−Cubic-structured europium (Eu) doped zinc sulfide (ZnS) nanoparticles (NPs) were prepared via refluxing at 150 °C. Absolute structural studies showed that Eu^+ ions were successfully substituted into the ZnS host lattice and changed the original structure of the host. As-fabricated ZnS:Eu NPs exhibited typical red emission due to the transition of the Eu dopant in the $^5d_0$-$^7f_1$, $^5d_0$-$^7f_2$, $^5d_0$-$^7f_3$, and $^5d_0$-$^7f_4$ energy levels of the 4f orbital of the dopant. The typical diamagnetic ZnS could be converted to tunable paramagnetic as a function of Eu-doping content. These NPs were quantified for hydrogen evolution through water splitting by artificial solar spectrum. Eu doping can drastically enhance the hydrogen (H_2) evolution capability of ZnS, which is higher than that of bare ZnS NPs. The causes behind these engrossing results will be revealed. These interesting properties may find applications in optoelectronics, spintronics, and H_2 evolution.

Keywords: ZnS, Dopant-induced, Photoluminescence; Paramagnetism; Hydrogen Evolution

INTRODUCTION

Nanocrystalline semiconductors are attracting more interest from researchers because of their possible applications in optoelectronics [1], biological labeling [2], spintronics [3], photocatalysis [4], and piezotronics [5]. Doped semiconductor nanostructures especially display several interesting properties compared to undoped nanostructures [6-10]. Recently, researchers have doped lanthanides into semiconductor compounds to alter their optical bandgap and photoluminescence properties [11]. Lanthanides with special 4f electrons have been explored as promising substances for luminescence centers in doped nanocrystalline semiconductors because they possess a unique 4f electronic structure related to the 5d-4f/4f-4f transitions that can establish engrossing emission features [12]. Among the various lanthanides, europium is the most often used candidate, because europium-doped nanostructures possess absorbing emission and magnetic properties.

Due to these leads, few researchers have reported on europium doped semiconductor compound systems. Mateus et al. [13] reported photoluminescence characteristics of Eu-doped ZnS nanoparticles through microwave-assisted solvothermal method and explained the correlation between theoretical and experimental calculations. Lotey et al. [14] reported the emission properties of ZnS : Eu nanoparticles. Ahemen et al. [15] observed the red emission in Eu doped ZnS nano phosphor with fluorescence efficiency. Sabit Horoz et al. [16] reported the magnetic as well as photovoltaic characteristics of ZnS : Eu quantum dots. Although, no meticulous studies are available on the europium doped ZnS systems. ZnS nanostructures are widely used as a promising host candidate and have distinctive optical, photoluminescence, and magnetic properties when mono-doped or co-doped with rare-earth elements [3,4]. These doped semiconductors are also called diluted magnetic semiconductors (DMSs), and they exhibit interesting magnetic properties at room temperature for spintronic applications. Moreover, doped ZnS nanostructures play a vital role in hydrogen (H_2) evolution under UV and visible illumination [4]. Based on the multifunctionality of the doped ZnS nanostructures, we can use a single material for different applications through suitable and sensible doping.

In the present study, Eu-doped ZnS NPs were successfully synthesized through a chemical refluxing route and achieved tunable bandgap, red emission, paramagnetism and enhanced H_2 evolution properties for optoelectronic, spintronic and H_2 evolution applications. Based on these interesting properties of the ZnS : Eu system, we strongly believe that this material is an all-round material that

†To whom correspondence should be addressed.
E-mail: ylkim@gwnu.ac.kr, sungjinan@kumoh.ac.kr, kipark@knu.ac.kr
‡These authors contributed equally to this work.

is a promising candidate for multifunctional applications.

EXPERIMENTAL AND CHARACTERIZATION

1. Materials

Zinc nitrate hexahydrate ($Zn(NO_3)_2 \cdot 6H_2O$), Sodium sulfide nonahydrate ($Na_2S \cdot 9H_2O$), Europium(III) nitrate pentahydrate ($Eu(NO_3)_3 \cdot 5H_2O$), and Ethylenediaminetetraacetic acid (EDTA). All are Merck products. Deionized water and Ethyl alcohol are the solvents.

2. Synthesis Procedure

Eu (0, 1, 3, and 5 at.%) doped ZnS nanoparticles (NPs) were prepared via a reflux technique. For bare ZnS, 0.03 M Zinc nitrate (0.3085 g) was mixed in 40 mL of deionized water beneath stirred at 50 °C. After that, 0.03 M of Na_2S (0.2882 g) was mixed in 40 mL of DI water and added to the zinc solution under continuous stirring. 0.2 g of EDTA was added to the ZnS solution as a stabilizer. The final solution was kept under refluxing for 5 h at 150 °C. The eventual precipitate was cleansed with ethyl alcohol several times and heated at 100 °C for 24 h. For the Eu (1 at.%, 3 at.%, and 5 at.%)-doped ZnS, 0.03 M Zinc nitrate (0.3498 g (1 at.%), 0.3355 g (3 at.%), and 0.3284 g (5 at.%)) and Europium nitrate (0.0102 g (1 at.%), 0.0205 g (3 at.%), and 0.0410 g (5 at.%)) were dissolved in 40 mL of DI water under stirring at 50 °C. The remaining process was like that of preparing the bare ZnS NPs.

3. Characterization

Particle size verification was done using a high resolution transmission electron microscope (HRTEM, Phillips TECHNAI FE 12) with an accelerating voltage of 200 kV. The structure of the nanoparticles was governed by X-ray diffraction (XRD) instrument with Cu-Kα radiation (λ=1.5406 Å) and the system was worked at 40 kV and 30 mA. Fourier transform infrared (FTIR) spectroscopy studies were recorded by FTIR-200 (Thermo Nicolet) equipment. An X-ray photo electron spectrometer (XPS, SPECS GmbH (Phoibos 100 MCD Energy Analyzer)) sophisticated instrument with Al Kα radiation having a residual pressure of the order of 2×10^{-8} Pa, was used to analyze the energy transition levels. Optical absorption was performed using double-beam spectrophotometer (Jasco V-670) for energy gap determination. Photoluminescence measurements were carried out using spectrometer (JOBIN YVON Fluorolog-3) consisting of a 450 W Xenon arc lamp as an excitation source. Magnetic characteristics of the prepared nanoparticles were studied through vibrating sample magnetometer (VSM) (Lakeshore 7410). The photocatalytic hydrogen evolution tests were carried out in a 150-ml quartz reactor at room temperature with an atmospheric

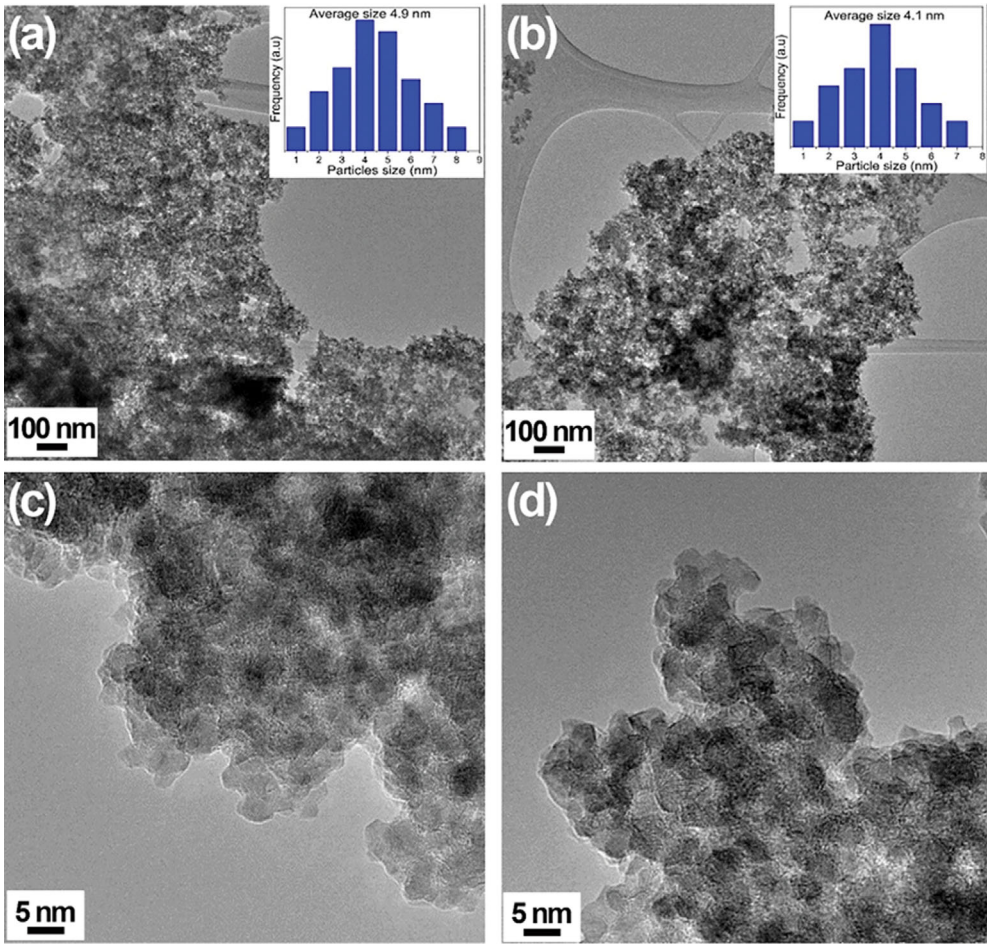

Fig. 1. (a), (b) transmission electron microscopy (TEM) with size distribution histograms (inset) and (c), (d) high-resolution TEM (HRTEM) images of ZnS : Eu (0 at.% and 5 at.%) NPs.

pressure. 5 mg of nanocatalysts was dissolved in 50 ml of aqueous solution containing 0.25 mol L^{-1} of Na_2SO_3 and Na_2S as electron donors. A 300-W (MaX 303 model) Xe lamp was used as a solar light (Intensity: 50 mW cm^{-2}) source. Before illumination, the reactor was evacuated by a vacuum pump and bubbled with N_2 for 20 min to remove the air inside the reactor. The produced H_2 gas was assessed via an off-line gas chromatograph (GC, YL-6500) equipped with a thermal conductivity detector and a 5-A molecular sieve column.

RESULTS AND DISCUSSION

Fig. 1 displays the ((a) and (b)) TEM images along with size distribution histograms (inset) and HRTEM images ((c) and (d)) of ZnS : Eu (0 at.% and 3 at.%) NPs. All the NPsare roughly spheroid shaped and slightly agglomerated. In general, nanoparticles have a higher respective surface area and higher comparative number of surface atoms. In particular, these atoms have unsaturated coordination and each atom consists of vacant coordinate sites. They attempt to make bonds and such bonds form between close to nanoparticles, this causes the agglomeration. In fact, very small nanoparticles (~5 nm) are feasibly difficult to observe separate nanoparticles. These are the common problems in nanoparticles for the case of agglomeration and aggregation [17]. No Eu content-dependent morphology was identified. The evaluated average diameter of the prepares nanoparticles was 4.9 and 4.1 nm for ZnS : Eu (0 at.% and 3 at.%) NPs, respectively. The nanoparticle size is examined and estimated by using the ImageJ software. Qu et al. [18] prepared

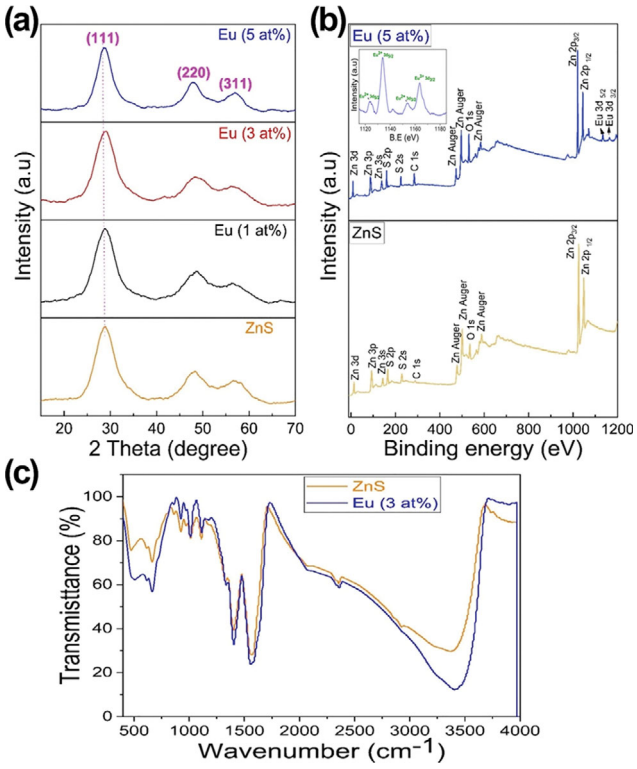

Fig. 2. (a) X-ray diffraction patterns, (b) XPS scan, and (c) Fourier-transform infrared spectra result of ZnS : Eu NPs.

monodispersed ZnS and Eu-doped ZnS nano-sized crystals through the co-precipitation reaction of inorganic precursors $ZnCl_2$, $EuCl_3$, and Na_2S in a water/methanol binary solution.

Fig. 2(a) illustrates the XRD patterns of ZnS : Eu NPs displaying typical (111), (200), (311), and (331) diffraction planes corresponding to the cubic structure of ZnS. The widening of the XRD peaks suggests that the fabricated samples are in the nano range. The penetration of Eu into the host matrix results in the diffraction peak moving slightly toward the lower angles, causing lattice amendment due to the mismatching atomic radii of Eu and Zn. The calculated values of the lattice constants occur in the range of 5.42-5.39 Å. The average diameter of the ZnS : Eu NPs was estimated from the full-width at half-maximum of diffraction level peaks through Debye-Scherer's formula, $D=0.89/\beta\cos\theta$. The crystalline size of the ZnS : Eu NPs was found in the range of 3.9-4.2 nm and was determined to decline with enhancing Eu content. This difference between the TEM and XRD results could be that the crystalline size in fact can be higher than that expected by the Debye-Scherrer formula with some additional peak width attributed from micro strains, which are common issue in tiny NPs. No supplementary peaks corresponding to foreign bodies were identified in the as-fabricated samples, which indicates that the NPs are single phase.

Fig. 2(b) represents the XPS spectra of the ZnS : Eu (0 and 5 at.%) NPs. The undoped samples reveal the existence of only Zn and S, however, in doped samples reveal Zn, S and Eu elements. For undoped ZnS NPs, zinc peaks were located at 1,022.07 and 1,043.18 eV, relative to Zn $2p_{3/2}$ and Zn $2p_{1/2}$, respectively. The sulfur peaks located at 161.98 eV and 162.95 eV, respectively, indicates the divalent state of sulfur. For, ZnS : Eu (5 at.%) NPs, two sharp peaks appear in the binding energy (B.E.) regions at 1,021.99 eV and 1,042.91 eV, which belong to Zn $2P_{3/2}$ and Zn $2P_{1/2}$, respectively. Two more peaks were found in the XPS spectra that belong to S 2P at 161.91 eV and 162.77 eV, revealing that sulfur ions exist in the material with a 2+ valence state. In addition, two peaks corresponding to the dopant ion were observed in the B.E. regions of 1,135.88 eV and 1,166.18 eV, which belong to Eu^{3+} $3d_{5/2}$ and Eu^{3+} $3d_{3/2}$ atomic factors. In addition, we also noticed the existence of a small fraction of Eu^{2+} ions with doublet positions at 1,125.9 and 1,157.8 eV (see the inset of Fig. 2(b)). Eventually, no extra peaks/foreign phases were found in the XPS spectrum of ZnS : Eu (5 at.%) NPs, indicating high-purity of the NPs. The elemental composition of undoped ZnS was Zn : S=51.31 : 48.69 and Eu doped ZnS was Zn : S : Eu= 46.87 : 49.24 : 03.89, which are nearer to the targeted values.

Fig. 2(c) displays the FTIR spectra of EDTA-passivated ZnS : Eu (0 at.% and 3 at.%) NPs. Wide absorption in the higher energy region at 3,345 cm^{-1} is noticed and is due to the -OH vibrations of water and EDTA, because all the studies employed mixing of NPs with KBr and it is well known that the KBr is hygroscopic [19]. The peaks at 1,558 cm^{-1} and 1,404 are associated with the antisymmetric and symmetric C=O stretching bands of the carboxylate anion related with EDTA. EDTA displays vibrational band at around 2,075 cm^{-1}, indicating that EDTA in a ZnS matrix forms a double betaine structure. The carboxylate ion groups are active in the catch EDTA in ZnS as evidenced by the noticed spectral bands at 1,558 and 1,404 cm^{-1}. The peak at 1,109 cm^{-1} is due to C-O stretching of

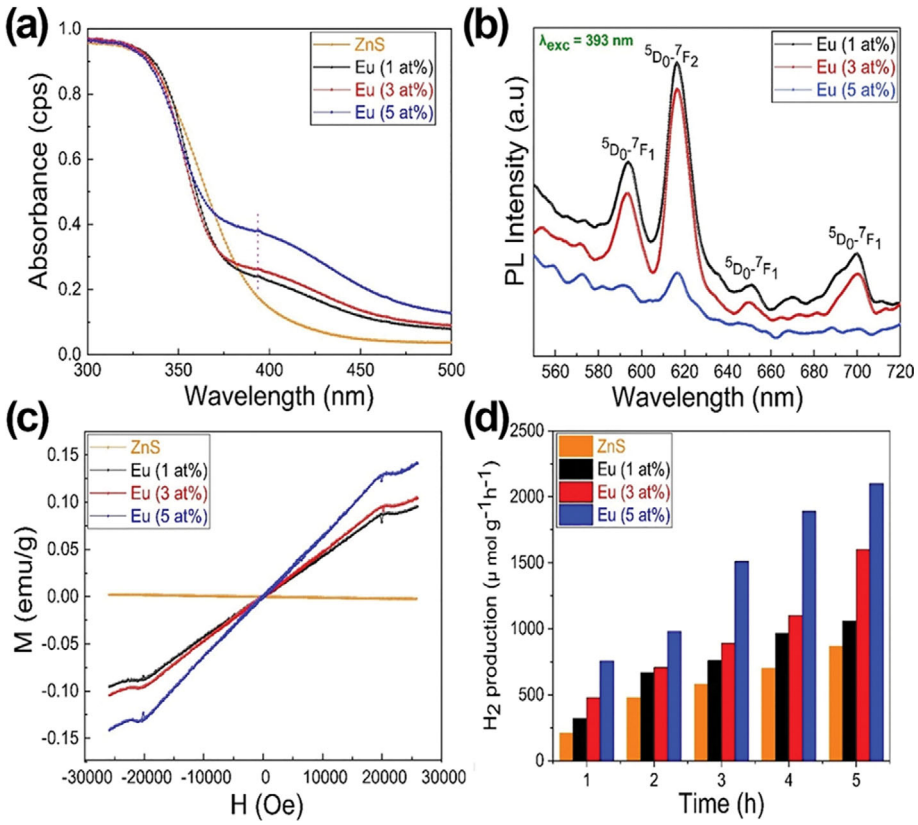

Fig. 3. ZnS : Eu NP results for (a) optical absorption, (b) photoluminescence, (c) vibrating sample magnetometry, and (d) H_2 evolution.

carboxylic acid. Ashwini et al. [20] noticed the presence of hydroxyl groups in the Eu doped ZnS nanoparticles. Moreover, the peaks at 472 cm^{-1} and 660 cm^{-1} are attributed to the zinc-sulfur stretching vibration. The FTIR spectra of the Eu-doped NPs found in the present investigation are like those of pure ZnS NPs. As is well known, the absence of extra peaks in the FTIR spectrum of Eu doped ZnS NPs indicates the impure free nature of the synthesized samples. This result suggests the successful incorporation of Eu into the ZnS matrix. This result is consistent with the previous report [19].

The ultraviolet-visible absorption spectra of the ZnS : Eu NPs are represented in Fig. 3(a). For the pure sample, the absorption edge observed at 330 nm (3.72 eV) is slightly bigger than that of the bulk ZnS band gap (3.67 eV), which is due to quantum confinement. The Eu-doped NPs display two absorption peaks at 330 nm and 393 nm. The second peak is ascribed to the $^7F_0 0^5L_6$ transitions of Eu (III) ions. In addition, the absorption peak of the Eu-doped NPs is shifted slightly toward the lower wavelength side with increasing Eu content because of the decreased size of the NPs. Fig. 3(b) displays the emission spectra of the Eu-doped samples (393-nm excitation). All these NPs exhibit four peaks at 593 nm, 616 nm, 650 nm, and 699 nm that are ascribed to the $^5D_0 \rightarrow {}^7F_1$ to $^7F_4$ electron transitions of the Eu (III) [21]. Moreover, we noticed a trivial decrease in fluorescence efficiency with increasing Eu content that emerges from the repeated excitation within the dopant sites and the thermal escape of transport carriers from confined states to other energy levels [22,23]. Lotey et al. [14] also observed five strong emission peaks at 574, 591, 617, 700, 754 nm in Eu-doped ZnS nanoparticles. Mou et al. [24] observed red emissions in Eu doped ZnS nanoparticles due to intra-4f transitions of Eu^{+3} ions under laser excitation (i.e., 374 nm), no characteristic red emission associated to 5 D_0-7 F_j (j=0, 1, 2,3, 4) transition of Eu^{+3} was found when excited with a laser wavelength of 325 nm. Recently, Poornaprakash et al. [25] noticed the emission spectra of ZnS : Eu QDs and displayed typical red fluorescence due to the transition of dopant ions in $^5D_0$-$^7F_1$, $^5D_0$-$^7F_2$, $^5D_0$-$^7F_3$, and $^5D_0$-$^7F_4$ energy levels of the 4f orbital of the Eu^{3+} ions.

Fig. 3(c) denotes the M-H hysteresis loops of the prepared samples. The pure NPs show the anticipated nonmagnetic behavior, whereas Eu-doped NPs exhibit typical paramagnetic characteristics at 300 K. Moreover, the paramagnetic behavior gradually enhances as a function of Eu content. First, the nonmagnetic behavior of the pure NPs is attributed to the lack of unpaired electrons that often occurs in II-VI semiconductor compounds [26]. Second, the obtained superparamagnetic character of the doped NPs owes its existence to the sporadic distribution of Eu ions in the host matrix that provoke weak interactions based on the gaps between the Eu ions and Eu concentration, thus impacting the power of direct or indirect solidity between the Eu ions. The enriched spontaneous magnetic moment found as a function of Eu doping indicates the number of spins enhanced with enhanced Eu doping and is a common phenomenon in transition metal/lanthanide-doped nanocrystalline semiconductor compounds [18]. Naohito et al. [27] reported the magnetic susceptibility features and disclosed the coexistence of Eu^{2+} and Eu^{3+} ions, though the existing

material contains only Eu^{3+} ions. Sabit Horoz et al. [16] reported that the Eu^{3+} doped ZnS samples exhibit signs of ferromagnetism; on the other hand, Eu^{2+} doped ZnS samples are paramagnetic of Curie-Weiss type. Poornaprakash et al. [28] observed the weak ferromagnetism in the Eu^{3+} doped ZnS nanoparticles.

Fig. 3(d) shows the H_2 production of the prepared samples via water splitting, which are 867 μmol $h^{-1}g^{-1}$, 1,059 μmol $h^{-1}g^{-1}$, 1,604 μmol $h^{-1}g^{-1}$, and 2,106 μmol $h^{-1}g^{-1}$ of H_2 in 5 h for ZnS : Eu (0 at.%, 1 at.%, 3 at.%, and 5 at.%). Thus, the H_2 production rate of ZnS : Eu (5 at.%) NPs is higher than that of pure ZnS NPs. A viable cause of the enhanced H_2 evolution of ZnS : Eu (5 at.%) NPs is the high surface area of the tiny particles. We believe that the tiny nanoparticle size would stimulate swift transport of photogenerated electrons, and the increased surface area would provide additional reaction sites, both of which can trigger enriched photocatalytic activity. In addition, diminishing fluorescence efficiency also decreases electron-hole recombination. These are possible reasons for enhanced H_2 evolution. Thus, Eu monodoping is a promising approach to extend the H_2 evolution capability of pure ZnS NPs. Recently, Poornaprakash et al. [25] reported the enhanced H_2 evolution properties as a function of increased Eu doping concentration ZnS quantum dots.

CONCLUSIONS

In summary, we have illustrated an easy Eu-doping way to significantly enrich the H_2 evolution capacity and red emission of ZnS NPs. XRD studies revealed that all the prepared NPs displayed a single-phase cubic structure like that of undoped ZnS. XPS analysis confirmed the existence and presence of Eu ions in the ZnS host in a trivalent state. The synthesized ZnS : Eu NPs have typical red emission behavior ascribed to the transition of Eu ions at the $^5D_0$-$^7F_{1\text{-}4}$ energy levels. The diamagnetic ZnS NPs turned into paramagnetic as a function of Europium doping concentration. The ZnS : Eu (5 at.%) NPs engendered the most H_2 evolution (2,106 μmol $h^{-1}g^{-1}$) in 5 h under artificial solar light illumination. These enticing properties of ZnS : Eu NPs have promising applications in optoelectronics, spintronics, and H_2 evolution.

ACKNOWLEDGEMENTS

This work was supported by the Technology Development Program (S3038568) funded by the Ministry of SMEs and Startups (MSS, Korea). This work also supported by the National Research Foundation of Korea funded by the Ministry of Science, ICT and Fusion Research (NRF-20201G1A1014959, NRF-2022R1I1A1 A01064248, 2021R1A4A2001658, and 2022R1A2C1003853). This work also supported by the National Research Foundation Korea funded by the Ministry of Science, ICT and Fusion Research (Grant No: 20201G1A1014959). Partially supported by NRF-2018R1A6 A1A03025761 and NRF-2018R1D1A1B07050766.

REFERENCES

1. Z. Y. Jiang, K. R. Zhu, Z. Q. Lin, S. W. Jin and G. Li, *Rare Met.*, **37**, 881 (2018).
2. H. Q. Huang, J. L. Liu, B. F. Han, C. C. Mi and S. K. Xu, *J. Lumin.*, **132**, 1003 (2012).
3. B. Poornaprakash, S. Ramu, K. Subramanyam, Y. L. Kim, M. Kumar and S. P. R. Mallem, *Ceram. Int.*, **47**, 18557 (2021).
4. B. Poornaprakash, U. Chalapathi, M. Kumar, S. Ramu, S. V. P. Vattikuti and S.-H. Park, *Mater. Lett.*, **273**, 127887 (2020).
5. P. Puneetha, S. P. R. Mallem, B. Poornaprakash, J.-H. Lee and J. Shim, *Nano Energy*, **84**, 105923 (2021).
6. C. Zhang, S. Liu, X. Liu, F. Deng, Y. Xiong and F. C. Tsai, *R. Soc. Open Sci.*, **5**, 171712 (2018).
7. G. T. Chavan, A. Sikora, N. B. Chaure, L. P. Deshmukh and C.-W. Jeon, *Mater. Lett.*, **320**, 132353 (2022).
8. G. T. Chavan, A. Yadav, B. Y. Fugare, N. M. Shinde, M. S. Tamboli, S. S. Kamble, A. Sikora, J. Warycha, B. J. Lokhande, S.-W. Kang, A. Kim and C.-W. Jeon, *J. Alloys Compd.*, **901**, 162822 (2022).
9. G. T. Chavan, A. Sikora, R. C. Pawar, J. Warycha, P. J. Morankar and C.-W. Jeon, *Ceram. Int.*, **49**, 282 (2022).
10. G. T. Chavan, N. M. Shinde, F. A. Sabah, S. S. Patil, A. Sikora, V. M. Prakshale, S. S. Kamble, N. B. Chaure, L. P. Deshmukh, A. Kim and C.-W. Jeon, *Appl. Surf. Sci.*, **574**, 151581 (2022).
11. A. A. Ansari, A. K. Parchur, B. Kumar and S. B. Rai, *J. Mater. Sci. Mater. Med.*, **27**, 178 (2016).
12. J. Y. Park, E. J. Jeon, Y. H. Choa and B. S. Kim, *J. Lumin.*, **208**, 145 (2019).
13. M. M. Ferrer, Y. V. B. Santana, C. W. Raubach, F. L. A. Porta, A. F. Gouveia, E. Longo and J. R. Sambrano, *J. Mol. Model.*, **20**, 2375 (2014).
14. G. S. Lotey, Z. Jindal, V. Singhi and N. K. Verma, *Mater. Sci. Semicond. Process.*, **16**, 2044 (2013).
15. I. Ahemen, K. Dilip and O. C. Melludu, *Adv. Sci. Eng. Med.*, **5**, 1188 (2013).
16. S. Horoz, B. Yakami, U. Poudyal, J. M. Pikal, W. Wang and J. Tang, *AIP Adv.*, **6**, 045119 (2016).
17. I. V. Beketov, A. P. Safronov, A. I. Medvedev, J. Alonso, G. V. Kurlyandskaya and S. M. Bhagat, *AIP Adv.*, **2**, 022154 (2012).
18. S. C. Qu, W. H. Zhou, F. Q. Liu, N. F. Chen and Z. G. Wang, *Appl. Phys. Lett.*, **80**, 3605 (2002).
19. D. A. Reddy, G. Murali, R. P. Vijayalakshmi and B. K. Reddy, *Appl. Phys. A*, **105**, 119 (2011).
20. K. Ashwini, C. Pandurangappa and B. M. Nagabhushana, *Phys. Scr.*, **85**, 065706 (2012).
21. Y. Wang, X. Liang, E. Liu, X. Hu and J. Fan, *Nanotechnology*, **26**, 375601 (2015).
22. V. Martyshkin, V. V. Fedorov, C. Kim, I. S. Moskalev and S. B. Mirov, *J. Opt.*, **12**, 024005 (2010).
23. H. Nelkowski and G. Grebe, *J. Lumin.*, **1-2**, 88 (1970).
24. M. Pal, N. R. Mathews, E. R. Morales, J. M. G. Jiménez and X. Mathew, *Opt. Mater.*, **35**, 2664 (2013).
25. B. Poornaprakash, S. V. P. Vattikuti, K. Subramanyam, R. Cheruku, K. C. Devarayapalli, Y. L. Kim, V. R. M. Reddy, H. Park and M. S. P. Reddy, *Ceram. Int.*, **47**, 28976 (2021).
26. B. Poornaprakash, D. A. Reddy, G. Murali, N. M. Rao, R. P. Vijayalakshmi and B. K. Reddy, *J. Alloys Compd.*, **577**, 79 (2013).
27. T. Naohito, K. Hideaki and K. Giyuu, *J. Appl. Phys.*, **93**, 6957 (2003).
28. B. Poornaprakash, P. T. Poojitha, U. Chalapathi and S. H. Park, *Mater. Lett.*, **181**, 227 (2016).